Optical and electrical properties of doped amorphous silicon suboxides

R. Janssen* and A. Janotta
Walter Schottky Institute, Technical University of Munich, Am Coulombwall, D-85748 Garching, Germany

D. Dimova-Malinovska
Central Laboratory for Solar Energy and New Energy Resources, Bulgarian Academy of Science, Tzarigradsko Chaussee 72, 1784 Sofia, Bulgaria

M. Stutzmann
Walter Schottky Institute, Technical University of Munich, Am Coulombwall, D-85748 Garching, Germany
(Received 5 March 1999; revised manuscript received 19 July 1999)

In this work we investigate the effects of thermal annealing on the optical and electrical properties of doped amorphous silicon suboxide (a-SiO_x:H) samples prepared by plasma-enhanced chemical-vapor deposition. Efficient *p*- and *n*-type doping is possible up to a concentration of 10 at. % oxygen. Structural properties of the films are deduced from hydrogen evolution measurements and infrared spectroscopy. Changes in the microscopic structure of the amorphous network upon thermal annealing at low annealing temperatures cause a dopant activation of the *p*-type samples. The resulting increase of the dark conductivity becomes less pronounced for increasing oxygen content of the films, but still comprises almost two orders of magnitude for samples with 9 at. % oxygen. *N*-type suboxides do not show such doping activation upon thermal annealing. Thermal annealing at higher temperatures leads to an effusion of hydrogen, reducing the optical band gap E_{04} of the samples. The dependence of E_{04} on the hydrogen content for amorphous suboxides with different oxygen content is investigated and found to be similar to that of amorphous silicon. [S0163-1829(99)03743-1]

I. INTRODUCTION

Hydrogenated amorphous silicon suboxides (a-SiO_x:H) represent a material system suitable for the application in silicon-based light-emitting devices. The optical band gap and stable room temperature photoluminescence can be controlled by varying the oxygen content of the films.[1,2] *P*- and *n*-type doping is possible by incorporation of boron and phosphorus into the films, and thus light-emitting diodes (LED) can be realized.[3,4] As previously shown, thermal annealing at temperatures below 300 °C significantly reduces the defect absorption of intrinsic suboxides and annealing of a-SiO_x:H *p-i-n* structures leads to a pronounced increase of the forward current densities and the total electroluminescence intensity.[5] This work was performed in order to better understand the effects of thermal annealing on *p*- and *n*-type suboxide layers with the aim to improve the performance and stability of a-SiO_x:H *p-i-n* structures.

II. EXPERIMENTAL DETAILS

P- and *n*-type a-SiO_x:H layers were deposited by plasma enhanced chemical-vapor deposition (PECVD) using SiH_4 (with 1 vol. % B_2H_6 or PH_3, respectively) and CO_2 as source gases and H_2 as dilution gas. The substrate temperature, deposition pressure and deposition power were nominally 250 °C, 0.5 mbar, and 1 W, respectively. The gas flow rates for SiH_4 and CO_2 were in the range of 1–8 sccm and the hydrogen dilution flow rate was 20 sccm. The oxygen content and the optical gap E_{04} (energy at which the absorption coefficient reaches values of $10^4\,cm^{-1}$) of the samples were controlled by varying the CO_2- partial pressure $CO_2/(SiH_4+CO_2)$ between 0 and 0.6.

Hydrogenated amorphous silicon (a-Si:H) deposited with our PECVD-system showed an optical band gap E_{04} of 1.95 eV, an Urbach energy of 70 meV, and a defect density of $10^{17}\,cm^{-3}$. The oxygen content of the suboxide films was determined by energy dispersive x-ray spectroscopy (EDX) using a silicon wafer and stoichiometric quartz as standards. The optical properties of a-SiO_x:H samples with variable oxygen content and thickness of approximately 1 μm deposited on Corning glass 7059 and quartz substrates were determined by transmission/reflection measurements and photothermal deflection spectroscopy (PDS). Electrical measurements were performed using coplanar evaporated Cr/Au contacts. To study the influence of annealing on the optical and electrical properties the samples were annealed under high vacuum ($p<10^{-6}$ mbar) or nitrogen atmosphere at temperatures between 200 °C and 900 °C. Additionally, hydrogen effusion spectra were measured by heating the films inside a quartz tube with a heating rate of 20 °C/min and measuring the H_2- partial pressure with a quadrupole mass spectrometer. Structural changes in the suboxide films caused by the thermal annealing were investigated by infrared (IR) spectroscopy performed with a Fourier transform IR spectrometer.

III. RESULTS AND DISCUSSION

A. Optical and structural properties

Figure 1 shows the optical band gap E_{04} as a function of the oxygen content for intrinsic, *p*- and *n*-type amorphous suboxides. For oxygen contents exceeding approx. 3 at. % a

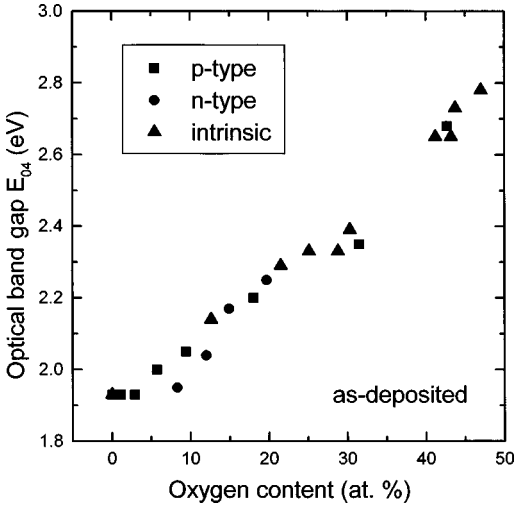

FIG. 1. Optical band gap E_{04} as a function of the oxygen content for doped and undoped a-SiO_x:H.

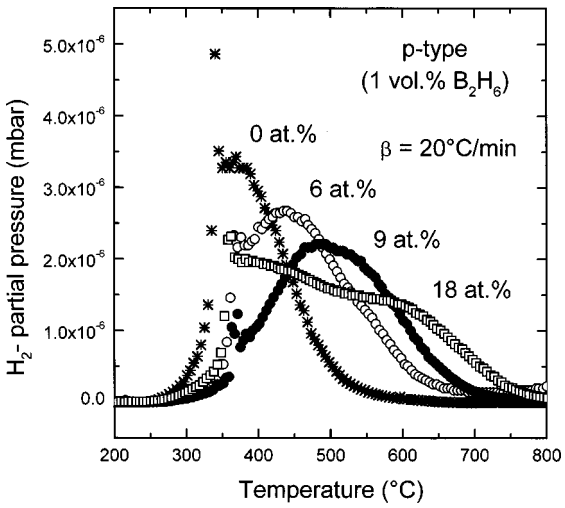

FIG. 2. Hydrogen effusion of p-type suboxides (1 vol. % B_2H_6) with oxygen contents of 0, 6, 9, and 18 at. % as a function of temperature.

linear increase of the optical bandgap is detected for both doped and intrinsic samples, and for an oxygen content of 50 at. % the optical band gap reaches a value of 2.8 eV. The mechanisms responsible for an increase of the optical band gap in a-SiO_x:H, when Si-Si bonds are replaced by Si-O-Si bridges, are discussed by Carius *et al.*[6] and should not be affected by the incorporation of dopant atoms. A theoretical study of the electronic structure of SiO_x by Martinez *et al.* confirmed a linear increase of the optical band gap for oxygen concentrations between 0 and 50 at. %.[7] Empirical results similar to our data for E_{04} as a function of the oxygen content were reported by Carius *et al.* for amorphous SiO_x alloys produced by glow discharge of SiH_4 and N_2O,[6] while dc magnetron sputtering using a crystalline silicon target and water vapor as the oxygen and hydrogen source results in samples with lower optical band gap due to the lower hydrogen content of the films.[8] The hydrogen content of magnetron sputtered samples was measured to be typically 10 at. %, whereas our samples have hydrogen concentrations exceeding 20 at. %. For comparison, our intrinsic a-Si:H with nominally 0 at. % oxygen has a hydrogen concentration of 15 at. %. The hydrogen is bound in Si-H configurations giving rise to a stretching vibration mode at 2000 cm^{-1} in the IR spectra.

The results of hydrogen effusion measurements of p-type suboxides (1% B_2H_6 diluted in SiH_4) are shown in Fig. 2. The total amount of effused hydrogen shows a slight increase with increasing oxygen content. The hydrogen content of samples with 0, 6, 9, and 18 at. % oxygen was 18, 20, 21, and 24 at. %, respectively. Up to 9 at. % oxygen there is a shift of the onset of hydrogen effusion and of the main effusion peak to higher temperatures, suggesting that back-bonded oxygen leads to stronger silicon-hydrogen bonding. It is assumed that all incorporated hydrogen is bonded to silicon, since IR spectroscopy gives no evidence for the existence of O-H bonds in amorphous silicon suboxides. The broadening of the effusion peaks with increasing oxygen content is caused by a larger variety of bonding environments. In contrast to the films with lower oxygen content the sample with 18 at. % oxygen shows a two peak effusion spectrum, with a low temperature effusion peak comprising for most of the bonded hydrogen. At oxygen contents exceeding 10 at. % a change in the microscopic structure of the boron-doped films leads to a different bonding environment of the incorporated hydrogen. All hydrogen has effused at temperatures exceeding 650 °C, 700 °C, 750 °C, and 800 °C for samples with 0, 6, 9, and 18 at. % oxygen, respectively. Note that at approximately 350 °C a spike appears in all effusion spectra. We will later return to this feature when discussing the change of the dark conductivity of p-type suboxides upon thermal annealing.

For comparison, Fig. 3 shows the hydrogen effusion spectra of n-type suboxides (1% PH_3 diluted in SiH_4). The effusion peak of n-type a-Si:H is shifted to higher temperatures by more than 100 °C with respect to the p-type a-Si:H. This agrees with earlier results by Beyer.[9] With increasing oxygen content again the high temperature effusion peak is shifted to higher temperatures due to increasing silicon-hydrogen bond energies and the amount of hydrogen in this bonding configuration is decreasing. The dominance of the low tempera-

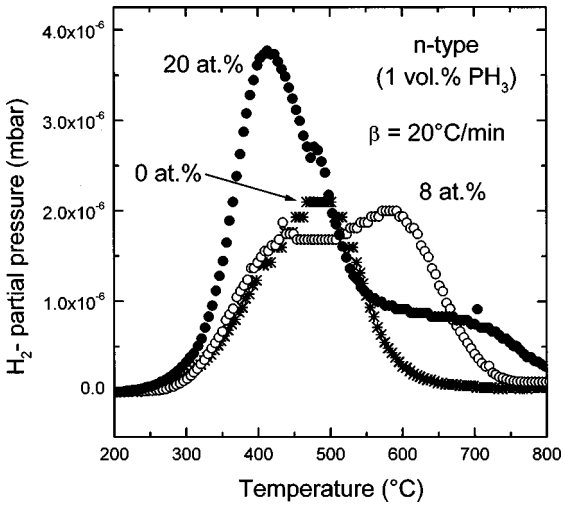

FIG. 3. Hydrogen effusion of n-type suboxides (1 vol. % PH_3) with oxygen contents of 0, 8, and 20 at. % as a function of temperature.

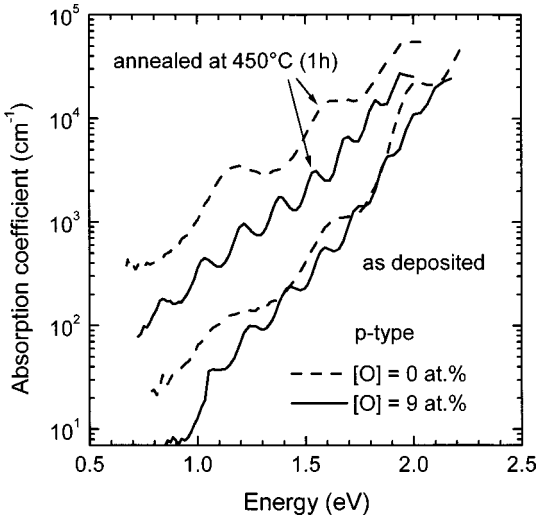

FIG. 4. Absorption coefficient of *p*-type suboxides with 0 and 9 at. % oxygen in the as-deposited state and after annealing at 450 °C (the structure observed is due to interference fringes).

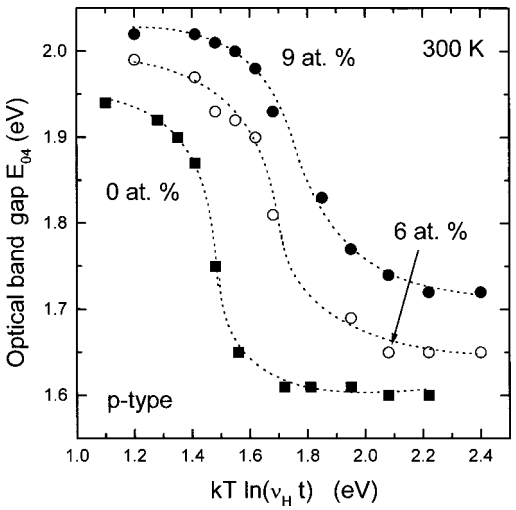

FIG. 5. Optical band gap E_{04} of *p*-type amorphous suboxides with oxygen contents of 0, 6, and 9 at. % as a function of an annealing energy parameter $E_{th}=kT\ln(\nu_H t)$. T and t are annealing temperature and time and $\nu_H=10^{10}$ Hz is a frequency prefactor commonly used for *a*-Si:H. The dotted lines are guides to the eye.

ture (LT) effusion peak for high oxygen contents again indicates a change in the bonding environment of the hydrogen. Note that for the *n*-type sample with 20 at. % oxygen the relative magnitude of the LT effusion peak is significantly larger than for the *p*-type sample with 18 at. % oxygen. We will later comment on this fact when discussing the dark conductivity of doped suboxides. After heating the *n*-type suboxides with 0, 8, and 20 at. % oxygen to 700 °C, 750 °C, and 850 °C, respectively, all hydrogen has effused from the samples. The total amount of hydrogen determined in this way was 16, 23, and 31 at. %, respectively. Both the high hydrogen content of more than 20 at. % and the formation of a low temperature effusion peak is a characteristic of void-rich amorphous silicon.[10] The most likely reaction accounting for the LT evolution peak is the rupture of two neighboring Si-H bonds simultaneous with the formation of H_2 and the subsequent rapid diffusion of molecular hydrogen through the open void-rich structure. The observation of an increasing dominance of the LT effusion peak with higher oxygen contents thus indicates an increasing concentration of voids in the films, both for *p*- and *n*-type amorphous suboxides. This fact was confirmed by electron micrographs of amorphous suboxides with high oxygen concentrations showing a void-rich structure.

We now focus on the effects of thermal annealing on the optical properties of *p*-type amorphous suboxides. The motivation for concentrating on doped layers with low oxygen content will be given in the following section on the electronic properties of amorphous suboxides, but briefly is due to the fact that doped layers determine the series resistance of *p-i-n* diodes. Figure 4 shows the absorption coefficient measured by photothermal deflection spectroscopy (PDS) for samples with 0 and 9 at. % oxygen in the as-deposited state and after thermal annealing at 450 °C for 1 h. For both samples thermal annealing reduces the optical band gap E_{04} and increases the Urbach energy and the sub-band-gap absorption due to the effusion of hydrogen. The reduction of the optical band gap is more pronounced for the sample with 0 at. % oxygen because at an annealing temperature of 450 °C a higher fraction of hydrogen has left the film (see Fig. 2).

Figure 5 shows the optical band gap E_{04} after consecutive annealing steps. All E_{04} data was taken from PDS spectra with an uncertainty of 0.01 eV. We introduce the parameter $kT\ln(\nu_H t)$ as a measure for the thermal annealing energy E_{th}, t and T being the annealing time and temperature, k the Boltzmann constant, and $\nu_H=10^{10}$ Hz a frequency prefactor commonly used for amorphous silicon.[11,12] In this case the frequency prefactor ν_H is describing an attempt-to-escape frequency for hydrogen effusion. For a thermally activated process with rate $\nu=1/t=\nu_0\exp(E_A/kT)$ one finds $E_A=kT\ln(\nu_0 t)$. Thus in a system with a distribution of activation energies, the energy parameter $E_{th}=kT\ln(\nu_0 t)$ separates systems which already have been thermally activated ($E_A<E_{th}$) from those which have not yet been affected ($E_A>E_{th}$). Therefore $kT\ln(\nu_0 t)$ is a useful parameter to combine isothermal and isochronal annealing experiments.

The values of E_{04} in the as-deposited state were 1.95, 1.98 and 2.02 eV and after effusion of all hydrogen 1.6, 1.65, and 1.72 eV for 0, 6, and 9 at. % oxygen, respectively. With increasing oxygen content the onset of the reduction of E_{04} is shifted to higher annealing energies and is spread out over a wider energy range, in good agreement with the hydrogen effusion spectra. In order to correlate the optical band gap measured after consecutive isochronal annealing steps with the hydrogen effusion spectra, the annealing energy parameter for the latter was calculated by discretizing the linear heating rate of 20 °C/min by subsequent annealing temperatures 5 °C apart and corresponding annealing times of 15 s. Figure 6 shows the effusion spectra presented in Fig. 2 as a function of the annealing energy parameter obtained in this manner. It is then possible to calculate the amount of effused hydrogen at a certain annealing energy and thus correlate the optical band gap with the hydrogen content of the films (Fig. 7). For all samples E_{04} increases approximately linearly with the hydrogen content. The explicit dependence of the optical

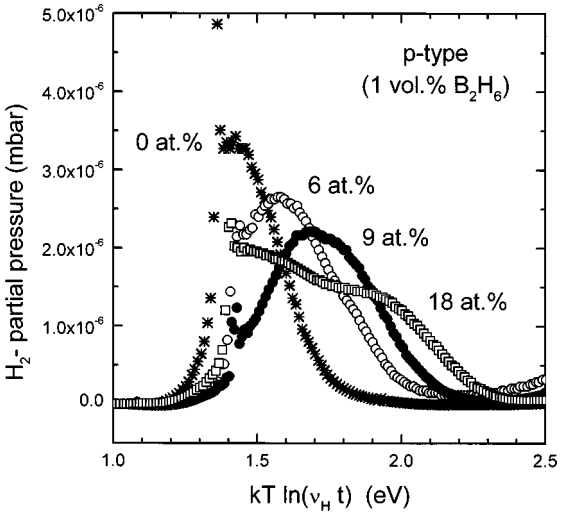

FIG. 6. Hydrogen effusion of *p*-type suboxides with oxygen contents of 0, 6, 9, and 18 at. % as a function of annealing energy.

band gap E_{04} on the hydrogen content [H] derived from linear least-square fits can be expressed in the form

$$E_{04}(\mathrm{H}) \approx E_{04}(0) + 0.02\,\mathrm{eV}\ [\mathrm{H}], \tag{1}$$

where [H] is given in at. % and E_{04} (0) is a function of the oxygen content, namely 1.60 eV, 1.66, and 1.73 eV for 0, 6, and 9 at. % oxygen, respectively. A similar dependence is usually observed for undoped *a*-Si:H[13] [$E_{04}(\mathrm{H}) \approx 1.67\,\mathrm{eV} + 0.02\,\mathrm{eV}\,[\mathrm{H}]$]. The somewhat lower value of E_{04} (0) for our samples with 0 at. % oxygen reflects the broadened band tail of doped compared to undoped samples, leading to smaller values of E_{04}.

According to photoemission measurements by von Roedern *et al.* performed on *a*-Si:H the dependence of the optical bandgap on the hydrogen concentration is mainly due to a recession of the top of the valence band of amorphous silicon by the transformation of Si-Si bonds into Si-H bonds.[14] For oxygen contents up to 10 at. % this mechanism seems to be

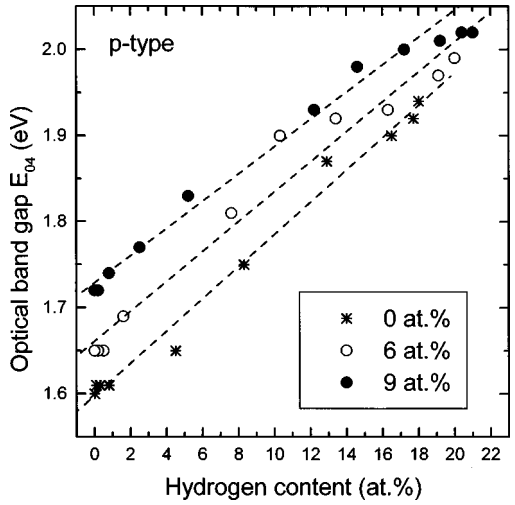

FIG. 7. Optical band gap E_{04} as a function of the hydrogen content for *p*-type suboxides with oxygen contents of 0, 6, and 9 at. %. The dashed lines are linear least square fits to the data.

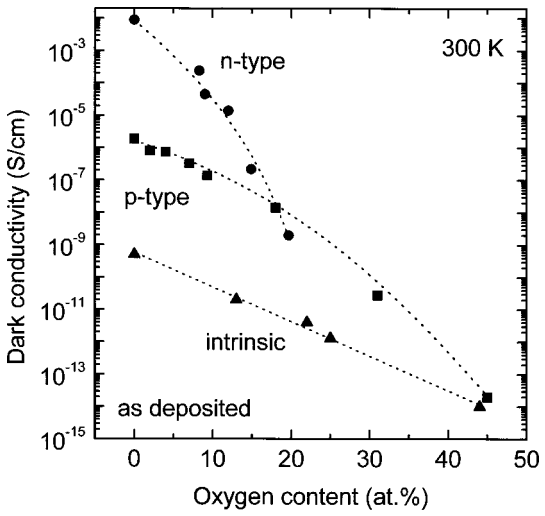

FIG. 8. Dark conductivity as a function of the oxygen content for as-deposited doped and undoped *a*-SiO_x:H. The dotted lines are guides to the eye.

valid for *p*-type suboxides as well, based on the comparable dependence of E_{04} on the hydrogen content.

B. Electrical properties

We now concentrate on the electrical properties of amorphous suboxides. Figure 8 shows the dark conductivity as a function of the oxygen content of the films for intrinsic, *p*- and *n*-type amorphous suboxides. Intrinsic samples exhibit a decreasing conductivity with increasing oxygen content corresponding to the larger optical band gap. This behavior is expected if the Fermi level is pinned close to the center of the band gap by dangling bond defects for all intrinsic samples. Dark conductivity values of 10^{-14} S/cm for intrinsic *a*-SiO_x:H with oxygen contents of ~40 at. % were also reported by Haga *et al.* for suboxides deposited by PECVD,[15] whereas sputtered samples show higher values by almost four orders of magnitude in the whole range of oxygen contents up to 45 at. %.[16] The latter is possibly caused by an increased contribution of hopping conductivity due to a higher defect density as deduced from subgap absorption. Efficient doping is possible up to ~10 at. % oxygen in the films, where *p*- and *n*-type doping enhances the conductivity by three and six orders of magnitude, respectively. For [O]<20 at. % the higher doping efficiency of *n*-type suboxides is explained in analogy to *a*-Si:H by a steeper conduction band tail compared to the valence band tail. Boron-doped *a*-SiO_x:H films with oxygen contents of 10 at. % (E_{04}=2.0 eV) and dark conductivities of 10^{-6} S/cm were reported by Ichikawa *et al.*.[17] The dark conductivity values of our boron-doped samples with 10 at. % oxygen are one order of magnitude lower in the as-deposited state, whereas the dark conductivity of 2×10^{-6} S/cm for our *p*-type as-deposited *a*-Si:H film is lower by almost two orders of magnitude compared to conductivity values for state-of-the-art *p*-type amorphous silicon.[18–20] Our conductivity values of 10^{-2} S/cm for *n*-type *a*-Si:H, on the other hand, agree well with published data for a phosphine concentration in the gas mixture of ~ 1 at. %.[18,19] One possible reason for the much lower conductivity of our *p*-type samples is that samples

used in this study with nominally [O]=0 at. % still contain a noticeable amount of oxygen contamination. It is known that oxygen acts as a donor in *a*-Si:H.[21–23] We therefore believe that a compensating effect of the oxygen contamination may contribute to the fact that only the dark conductivity of our *p*-type samples is significantly reduced. A compensation of boron and oxygen in amorphous silicon was reported by Isomura *et al.*[24] They showed that boron concentrations of $10^{17}\,\mathrm{cm}^{-3}$ lead to a full compensation of oxygen concentrations in the range of $10^{20}\,\mathrm{cm}^{-3}$. The physical origin of the electrically active oxygen related states (donor states) has so far not been agreed upon. Shimizu *et al.* suggested the existence of positively charged, threefold-coordinated oxygen atoms (O_3^+),[22,25] whereas Pontushka *et al.* favored positively charged, singly coordinated oxygen atoms.[26] It should also be noted that oxygen gives rise to a large number of shallow donor levels in crystalline silicon (thermal donors, new donors) whose exact microscopic structure has not yet been established.

A further possible reason for the significantly lower dark conductivity values of our *p*-type samples is the passivation of boron acceptors by hydrogen atoms due to the formation of boron-hydrogen complexes.[36–38] The effect of hydrogen evolution and a subsequent reconstruction of the amorphous network caused by thermal annealing on the dark conductivity of *p*-type suboxides will be discussed further below.

With increasing oxygen content the probability for the incorporation of dopant atoms at electrically inactive sites is greatly enhanced and consequently the dark conductivity of both *p*- and *n*-type suboxides is diminished, until for the *p*-type sample with 45 at. % oxygen no doping effect can be detected. At such high oxygen concentrations the probability of the formation of active dopant sites (dopant atom surrounded by four silicon atoms) is at least one order of magnitude smaller than for low oxygen contents, based on continuous random network statistics alone. A reduction of the dark conductivity was also detected for amorphous films exhibiting a void-rich microstructure. Beyer reported a conductivity decrease for *n*-type *a*-Si:H with hydrogen concentrations exceeding 20 at. % which could be correlated with the presence of a low temperature effusion peak.[10] A comparison with Figs. 2 and 3 shows that a LT effusion peak appears for our *p*-type samples with [O]>10 at. % and that the LT effusion peak is more pronounced for *n*-type (as compared to *p*-type) suboxides at oxygen contents below 20 at. %. We therefore believe that an increasing concentration of voids also contributes to the strong reduction of the dark conductivity of our doped suboxides with rising oxygen content. The relatively larger conductivity decrease of our *n*-type samples (see Fig. 8) in this context can be explained by an even higher concentration of microvoids in agreement with the dominance of the LT effusion peak in these samples. For oxygen concentrations of $\sim$ 20 at. % the dark conductivity of both *p*- and *n*-type amorphous suboxides amounts to about the same low value of 10^{-8} S/cm.

One goal of our research work done on amorphous suboxides is the fabrication of light emitting *p*-*i*-*n* diodes. As intrinsic suboxides show a maximum of the room temperature photoluminescence intensity at $\sim$40 at. % oxygen,[27] it appears favorable to incorporate oxygen into the doped layers in order to enhance their optical bandgap and thus minimize the band gap discontinuities at the interfaces of the *p*-*i*-*n* structures. Particularly the *p*-*i* interface, i.e., the injection of holes in the intrinsic layer, seems to be of critical importance for the electroluminescence properties of amorphous silicon suboxide light emitting diodes.[28] On the other hand, the low conductivity of the *p*-type layer—as compared to the *n*-type layer—for [O]<10 at. % determines the series resistance of the *p*-*i*-*n* diodes at high applied forward voltages and thus limits the current density at a given voltage.[5] As both a high current density and an efficient injection of holes in the *i* layer are crucial for the electroluminescence properties, it is therefore necessary to apply *p* layers with the best compromise between optical band gap and dark conductivity in the *p*-*i*-*n* structures.

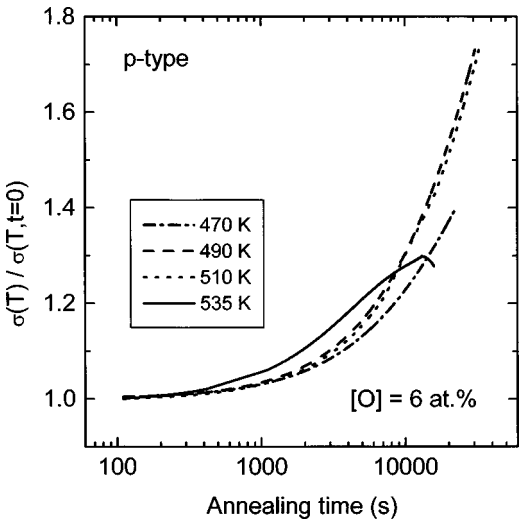

FIG. 9. Normalized dark conductivity as a function of annealing time at annealing temperatures of 470, 490, 510, and 535 K for a *p*-type suboxide with 6 at. % oxygen.

Thermal annealing at low temperatures ($T<550$ K) leads to a significant, irreversible increase of the dark conductivity of *p*-type suboxides. As an example Fig. 9 shows the effect of thermal annealing on the normalized dark conductivity of a *p*-type sample with 6 at. % oxygen for annealing temperatures between 470 and 535 K. Thermal annealing for about 6 h at temperatures as low as 470 K already causes an enhancement of the dark conductivity by a factor of 1.4. At longer annealing times t a logarithmic dependence of $\sigma(t)$ was observed. An accelerated activation of the dark conductivity can be realized by increasing the annealing temperature. At 535 K, conductivity activation was only found up to annealing times of 4 h, where σ passes through a maximum and decreases again for longer t. Thermal activation of the dark conductivity of our *p*-type suboxides is thus only possible in a limited range of annealing temperatures and times.

Figure 10 shows the dark conductivity of *p*-type samples measured at room temperature after consecutive annealing steps at increasing temperatures. As a measure for the thermal annealing energy we used the parameter $kT\ln(\nu_\sigma t)$, where ν_σ is a frequency prefactor characteristic for the structural changes affecting the electrical properties of amorphous silicon suboxides upon thermal annealing. To a first approximation we can assume the frequency prefactor ν_σ to be equal to ν_H (frequency prefactor for hydrogen effusion), although in general different microscopic processes will be at the ori-

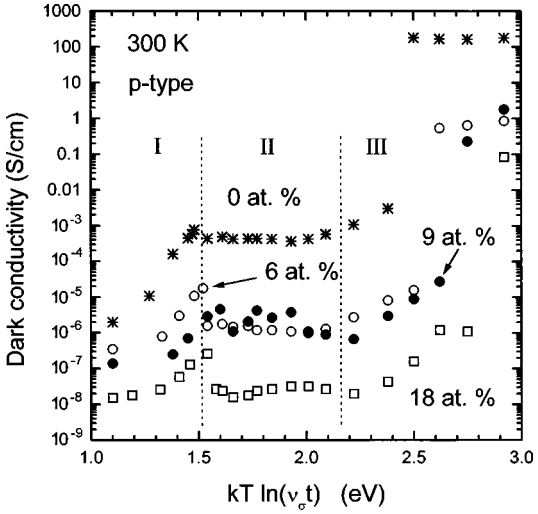

FIG. 10. Room temperature dark conductivity of *p*-type suboxides with oxygen contents of 0, 6, 9, and 18 at. % as a function of annealing energy (Regions I–III are described in the text.)

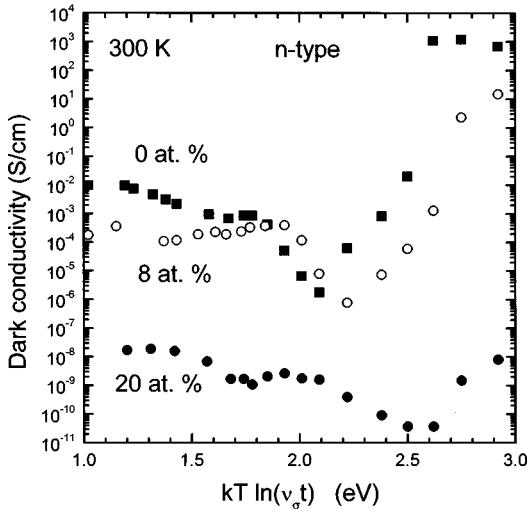

FIG. 11. Room temperature dark conductivity of *n*-type suboxides with oxygen contents of 0, 8, and 20 at. % as a function of annealing energy.

gin of hydrogen effusion and the variation of electrical properties of amorphous suboxides.

An enhancement of the dark conductivity of *p*-type samples was observed for annealing energies lower than 1.5–1.6 eV (corresponding to the 4-h annealing at 535 K shown in Fig. 9 or an equivalent 1 h annealing at 550 K, regime I). It is most prominent for the *a*-Si:H sample where it leads to an increase of the dark conductivity by almost three orders of magnitude. With larger oxygen content the doping activation is reduced, but still comprises more than one order of magnitude at 18 at. % oxygen.

At annealing energies of approximately 1.5 eV a sharp drop occurs in the dark conductivity by about one order of magnitude for all *p*-type samples containing oxygen. We believe that the origin of this conductivity reduction is the sudden effusion of a specific subset of hydrogen indicated by the spikes in the hydrogen effusion spectra at low temperature (see Fig. 6). A correlation of these two characteristic features will be discussed below. After the sharp drop the dark conductivity remains almost unchanged over a wide range of annealing energies for all samples (regime II). This is quite remarkable in view of the fact that the majority of the incorporated hydrogen effuses from the films in this annealing regime (see Fig. 6), however apparently without any effect on the dark conductivity, although the defect density increases notably (see Fig. 4). A slight increase of the dark conductivity indicating partial crystallization of the films (regime III) is followed by an increase of several orders of magnitude due to total crystallization of the films. Note that both the onset of crystallization and the total crystallization are shifted to higher annealing energies with increasing oxygen content. Comparison with Fig. 6 shows that the onset of crystallization is detected only after all hydrogen has effused from the films.

The dark conductivity of *n*-type suboxides as a function of the thermal annealing energy is shown in Fig. 11. Instead of a conductivity activation, detected for *p*-type samples, the dark conductivity decreases slowly (or remains approximately constant for the sample with 8 at. % oxygen) until there is a significant decrease of the dark conductivity at annealing energy values of 1.8 to 2.1 eV. This sharp drop corresponds to the high temperature peak of the hydrogen effusion spectra of *n*-type samples. Thus the breaking of strong silicon-hydrogen bonds results in a significant reduction of the dark conductivity. After total effusion of hydrogen from the films partial crystallization of the films is detected, leading to an increase in the dark conductivity. Total crystallization was reached for *n*-type samples with 0 and 8 at. % oxygen at annealing energies of 2.6 and 2.9 eV (corresponding to a 1-h anneal at 690 °C and 800 °C), respectively, whereas it was not possible to fully crystallize the sample with 20 at. % oxygen for annealing temperatures up to 900 °C.

C. IR transmission spectroscopy

To clarify the structural changes of *p*-type amorphous suboxides upon thermal annealing IR transmission measurements were performed. Figures 12(a) and 12(b) show IR transmittance spectra between 500 and 2500 cm^{-1} for samples with 0 and 9 at. % oxygen after consecutive annealing steps. Both spectra show the well-known Si-H wagging mode at 640 cm^{-1} decreasing in intensity as hydrogen effuses from the samples until all hydrogen has disappeared for $E_{th}=1.8$ eV. The structure appearing at 600 cm^{-1} is due to two-phonon absorption in the *c*-Si substrate,[29] The sample with 0 at. % oxygen also exhibits the $Si\text{-}H_2$ scissors vibration at 880 cm^{-1} and a very weak mode at 840 cm^{-1} attributed to the wagging mode of polysilanes $(Si\text{-}H_2)_n$ in the as-deposited state[30] [Fig. 12(a)]. We thus assume that $Si\text{-}H_2$ and—to a lesser extent—$(Si\text{-}H_2)_n$ configurations are present in our untreated films. These features vanish at an annealing energy of 1.35 eV, closely corresponding to the spike observed in the effusion spectra (see Fig. 6). We attribute this sudden effusion to weakly bound hydrogen including $Si\text{-}H_2$ and $(Si\text{-}H_2)_n$ configurations. After this effusion a restructuring of the network is likely to occur leading to the observed changes in the conductivity properties of the material. The corresponding stretching vibrations of Si-H and $Si\text{-}H_2$ groups appear at 2000 and 2090 cm^{-1}, respectively. At annealing

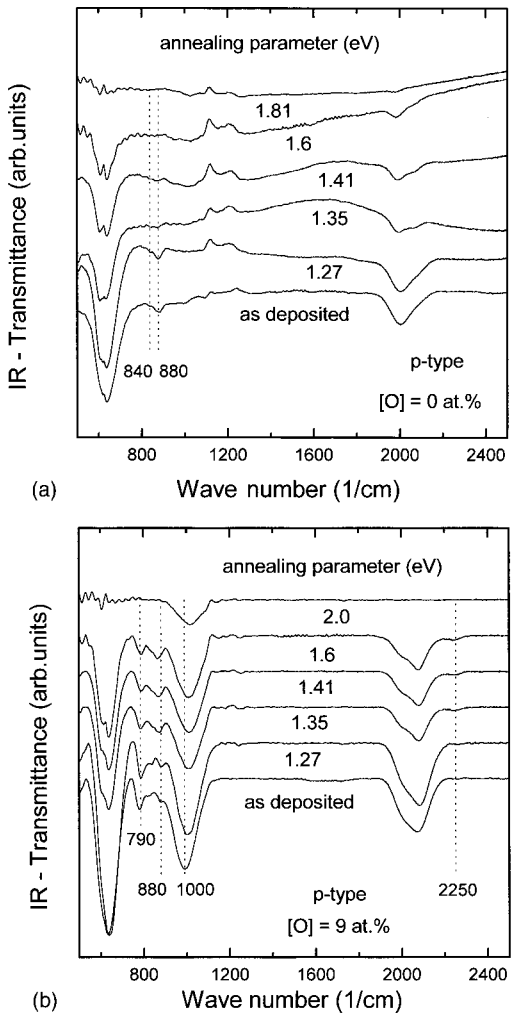

FIG. 12. IR transmittance spectra of *p*-type suboxides after annealing steps at successively increasing annealing energies. The dotted lines indicate vibrational modes described in the text. (a) [O]=0 at.%. (b) [O]=9 at.%

energies exceeding 1.35 eV we indeed detect a reduced absorption ratio of 2090 cm^{-1}/2000 cm^{-1} indicating a reduction of hydrogen bonded as dihydride. However, even after the total disappearance of the Si-H_2 scissors mode at 880 cm^{-1} there still remains a noticeable contribution of the 2090 cm^{-1} mode to the stretching vibrations. In accordance with earlier work we explain this fact by a fraction of monohydride bonds situated in larger cavities or in microscopic voids. It was shown by Cardona,[29] that the presence of Si-H bonds at the surface of internal voids leads to a shift of the stretching frequency from 2000 cm^{-1} to approximately 2100 cm^{-1}. We thus have evidence that in our sample with 0 at.% oxygen annealing energies of up to 1.35 eV lead to an effusion of weakly bound hydrogen from Si-H_2 and $(Si\text{-}H_2)_n$ configurations resulting in an amorphous material with internal voids. It has to be noted that the features in the IR spectra appearing around 1100 cm^{-1} are due to the *c*-Si substrate and that no evidence for unintentional incorporation of oxygen in the films during the annealing process was observed.

The IR spectra of the sample with 9 at.% oxygen are more complex [see Fig. 12(b)]. In the as-deposited state, two additional features are observed in the spectral region between 750 and 1100 cm^{-1}. The absorption band centered at around 790 cm^{-1} has been assigned to an overlap of a local bond configuration with mixed bending and stretching character for oxygen and hydrogen atoms bonded to the same silicon atom at 780 cm^{-1} (Ref. 31) and of the Si-O bending mode at 810 cm^{-1} (Ref. 32). Evidence for the contribution of hydrogen to this mode is given by its disappearance after the total effusion of hydrogen at annealing energies of 2.0 eV. The absorption band centered at 1000 cm^{-1} is the well-known Si-O-Si stretching mode that was shown to shift to higher wave numbers with increasing oxygen content.[33] At annealing parameters exceeding 1.27 eV the Si-O-Si stretching mode indeed exhibits such a slight shift to higher wavenumbers. This fact can be explained by the onset of phase separation of the suboxide into Si and SiO_2, leading to an enhanced concentration of oxygen in some parts of the film. As far as Si-H stretching modes are concerned, there are four distinct local environments for the Si-H group in amorphous suboxides. These can be written as $HSi\text{-}Si_{3-n}O_n$ with $n=0,\ldots,3$. The corresponding Si-H stretching frequencies are 2000, 2100, 2195, and 2265 cm^{-1}.[32] Our as-deposited sample with 9 at.% oxygen shows contributions at 2000 and 2100 cm^{-1} indicative of configurations with zero and one backbonded oxygen atom. Naturally an analysis of this spectral region is complicated, as Si-H_2 and $(Si\text{-}H_2)_n$ vibrations overlap the $HSi\text{-}Si_{3-n}O_n$ modes. Nevertheless, at annealing parameters exceeding 1.35 eV an additional mode at 2250 cm^{-1} becomes visible. This mode is due to the HSi-O_3 stretching vibration and provides further evidence for a restructuring of amorphous suboxides into a silicon-rich and an oxygen-rich phase. Additional proof for this is a small, but noticeable shift of the mode at 880 cm^{-1} to lower wave numbers at 875 cm^{-1}. The latter mode has been identified as the bending mode of HSi-O_3.[32] We thus interpret this change in the IR spectra at annealing energies of 1.35 eV as the disappearance of the Si-H_2 scissors mode—which was also detected for our sample with 0 at.% oxygen—accompanied by the emergence of the HSi-O_3 bending mode. Again the hydrogen-related nature of the mode at 875 cm^{-1} was confirmed by the disappearance of the mode at annealing energies of 2.0 eV.

Thus annealing of the *p*-type sample with 9 at.% oxygen causes the following changes in the amorphous structure. At low annealing energies weakly bound hydrogen (e.g., Si-H_2) effuses from the film, and a concomitant restructuring of the amorphous network leading to an agglomeration of oxygen and possibly a phase separation into a silicon-rich and an oxygen-rich phase takes place. This phenomenon of phase separation in amorphous suboxides was also reported by Haga *et al.* for as-deposited undoped films with oxygen concentrations between 9 and 60 at.% prepared by rf glow discharge decomposition of SiH_4-CO_2 gas mixtures.[34] Finally, we would like to state that no local modes attributed to boron vibrations [such as the B-H stretching mode at 2560 cm^{-1} and the B-O stretching mode at 1350 cm^{-1} (Ref. 35)] could be detected in our *p*-type samples. Moreover, there was no evidence for the characteristic hydrogen vibration at 1875 cm^{-1}, correlated with B-H complexes responsible for an acceptor passivation in boron-doped crystalline silicon.[36–38]

A comparison of Figs. 6 and 10 shows that the annealing energy at which the effusion spike and the structural changes observed by IR spectroscopy occurs is lower by approxi-

mately 0.12 eV compared to the annealing energy of the drop in the conductivity. A correlation of the effusion spike and the conductivity drop can thus be achieved by assuming a ratio of the frequency prefactors $\nu_H/\nu_\sigma \approx 10$. Such different values for the frequency prefactors ν_H and ν_σ can be explained by the assumption that one out of ten hydrogen atoms which are effused from the sample at low annealing energies causes a change in the electrical properties of the amorphous suboxides. In the range of thermal conductivity activation [i.e., $kT\ln(\nu_\sigma t) < 1.5-1.6$ eV, regime I] $\sim$ 2 at. % of weakly bound hydrogen atoms effuse from the films. We therefore assume that the activation of boron acceptors is either directly caused by removal of hydrogen atoms or is mediated by a small scale motion of hydrogen. The exact physical process leading to an enhanced incorporation of electrically active, fourfold coordinated boron atoms is not known, as IR spectra give no evidence for boron-hydrogen complexes prior to thermal annealing. We will show later that the increase of the active acceptor density corresponds to $4\ 10^{19}\ \mathrm{cm}^{-3}$ at most. Such small changes in the concentration of hydrogen bonds are below the detection limit of our present IR-analysis, so that no direct microscopic evidence is available so far.

D. Temperature-dependent dark conductivity

The influence of the hydrogen effusion and the reconstruction of the amorphous network on the conductivity of *p*-type suboxides can be further investigated by measuring the temperature dependence of the dark conductivity. Figures 13(a) and 13(b) show the Arrhenius plot of the temperature dependent dark conductivity for a *p*-type sample with 9 at. % oxygen after various annealing steps. The conductivity is thermally activated for temperatures exceeding 370 K and is described by

$$\sigma(T) = \sigma_0 \exp(-E_\sigma/kT), \tag{2}$$

where σ_0 is the conductivity prefactor and $E_\sigma = E_F - E_V$ the activation energy (Fermi energy E_F, valence-band energy E_V). The range of thermal conductivity activation at low E_{th} (see Fig. 10, regime I) is displayed in Fig. 13(a). An increase of the annealing energy from 1.1 eV to 1.45 eV and 1.6 eV causes a reduction of E_σ from 0.73 eV to 0.66 eV and 0.56 eV, respectively. At the same time σ_0 decreases from 7×10^4 S/cm to 2×10^4 S/cm and 5×10^3 S/cm, respectively. The increase of the dark conductivity at 300 K is thus due to a shift of the Fermi energy towards the valence band edge. As for $kT\ln(\nu_0 t) < 1.6$ eV [i.e., $kT\ln(\nu_H t) < 1.48$ eV in Fig. 5] the reduction of the optical bandgap is negligible, the decrease of E_σ is caused by an activation of boron acceptors. A quantitative analysis of this effect will be presented below.

In Fig. 13(b) the $\sigma(T)$ data at $E_{\mathrm{th}} = 1.85$ and 2.4 eV represent the regime II of constant dark conductivity after the sharp conductivity drop and the regime III of partial crystallization, respectively (see Fig. 10). The lower conductivity at 300 K for $E_{\mathrm{th}} = 1.85$ eV as compared to $E_{\mathrm{th}} = 1.6$ eV is caused by a significant reduction of σ_0 from 5 10^3 S/cm to 5 10^2 S/cm. The observed small decrease of E_σ to 0.53 eV is probably due to the diminishing optical band gap (cf. Fig. 5). After the onset of partial crystallization ($E_{\mathrm{th}} = 2.4$ eV) σ at 300 K increases again: a further decrease of σ_0 is accompanied by a large reduction of E_σ to 0.38 eV. In nanocrystalline silicon the doping efficiency of boron is close to unity. The resulting increase of electrically active acceptors will then lead to a further shift of the Fermi level closer to the valence band, until finally degenerate *p*-type conduction is observed for full crystallization.

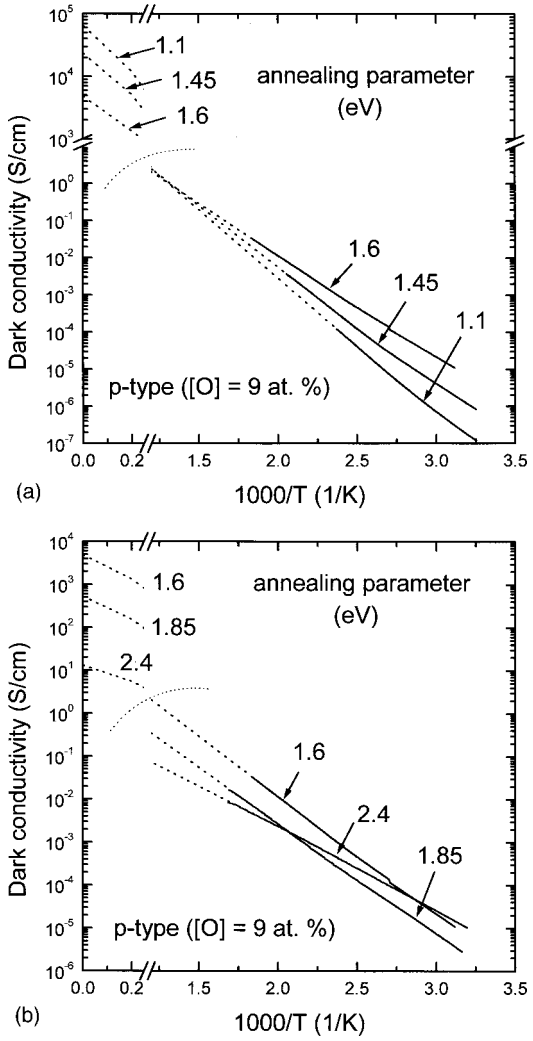

FIG. 13. Temperature-dependent dark conductivity after various annealing steps for a *p*-type suboxide with 9 at. % oxygen. (a) Low annealing energy parameters: $E_{\mathrm{th}} = 1.1-1.6$ eV. (b) High annealing energy parameters: $E_{\mathrm{th}} = 1.6-2.4$ eV. The dotted lines are extrapolations of the experimental data giving the value of the conductivity prefactor σ_0 at the intercept with the *y* axis (see top left corner of the figures).

For a further discussion of the temperature dependent dark conductivity we have used the correlation between the conductivity prefactor σ_0 and the activation energy E_σ (Meyer-Neldel rule). Figure 14 shows a Meyer-Neldel plot ($\ln\sigma_0$ as a function of E_σ) for *p*-type suboxides with 0 and 9 at. % oxygen. Both samples clearly exhibit the existence of three distinct regimes (indicated in Fig. 14 for the sample with 9 at. % oxygen). These correspond to the regimes (shown in Fig. 10) of the thermally activated dark conductivity ($E_{\mathrm{th}} < 1.5-1.6$ eV, regime I), the constant dark conductivity after the sharp conductivity drop ($1.5-1.6\ \mathrm{eV} < E_{\mathrm{th}} < 2.0-2.2$ eV, regime II) and the partial

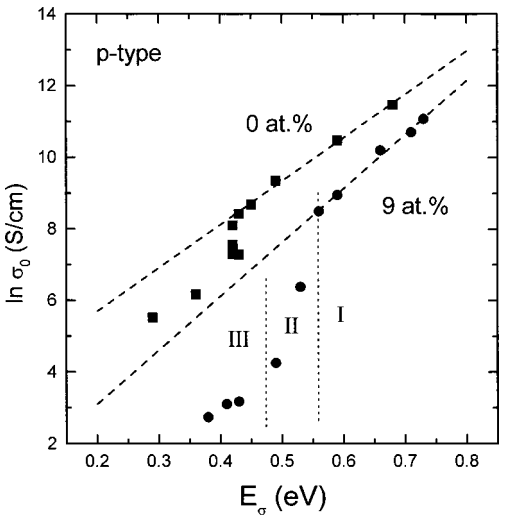

FIG. 14. Conductivity prefactor σ_0 vs the conductivity activation energy E_σ for *p*-type suboxides with 0 and 9 at. % oxygen. The dashed lines represent the Meyer-Neldel relations (Regions I–III indicated for the sample with 9 at. % oxygen are described in the text.)

crystallization ($E_{\text{th}}>2.0$–2.2 eV, regime III). For large activation energies (regime I) the data can be described by the Meyer-Neldel relation

$$\ln \sigma_0 = \ln \sigma_{00} + E_\sigma / kT_m , \tag{3}$$

where for our samples with 0 (9) at. % oxygen, σ_{00} is a constant with a value of about 25 (1) $\Omega^{-1}\,\text{cm}^{-1}$ and kT_m equals 83 (66) meV, respectively.

The Meyer-Neldel relation states that the temperature dependent conductivity data for different samples (in our case: a sample after different annealing steps) all intersect at the same value of the conductivity, σ_{00}, at the temperature T_m. A comparison with Figs. 13(a) and b shows that this is observed for the sample with 9 at. % oxygen only up to annealing energies of 1.6 eV, the value of T_m being 770 K. A departure of the data from the straight line in Fig. 14 (regime II) for activation energies lower than 0.6 eV is caused by a significant reduction of the conductivity prefactor. Similarly, the sample with 0 at. % oxygen follows the Meyer-Neldel relation only down to activation energies of 0.4 eV. For both samples the transition from regime I to regime II occurs at annealing energies of 1.5–1.6 eV, corresponding to the detected drop in the conductivity (see Fig. 10). We have shown in the previous section that the conductivity drop can be correlated with the sudden effusion of weakly bound hydrogen followed by a reconstruction of the amorphous network. We therefore believe that the observed reduction of the conductivity prefactor is caused by percolation effects in the amorphous films. IR measurements have given evidence that after the sudden effusion of hydrogen the *p*-type sample with 0 at. % oxygen consists of a void-rich material and the *p*-type sample with 9 at. % oxygen exhibits an agglomeration of oxygen. Both structural changes result in a phase separation leading to one phase with a higher and one phase with a lower conductivity. The current will thus be forced to percolate through the high conductivity phase and the reduction of the active sample volume contributing to the current transport is the reason for the strong decrease of the conductivity prefactor. With the onset of partial crystallization (regime III) the strong reduction of σ_0 comes to an end and the data again essentially follow a Meyer-Neldel relation.

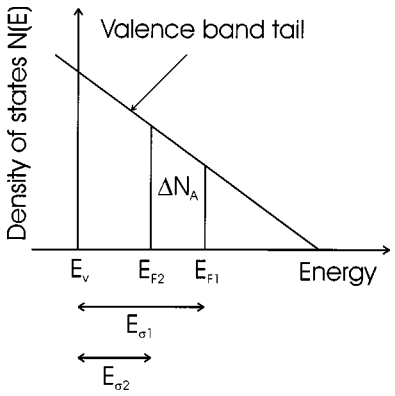

FIG. 15. Schematic diagram showing the shift of the Fermi level due to a filling of the valence band tail states by activated dopants.

Finally, we would like to state that all activation energy and conductivity prefactor values in Fig. 14 were deduced from the slope of the temperature dependent dark conductivity. We have not used the theoretically derived constant value of approximately 200 S/cm for the conductivity prefactor σ_0 (Ref. 39) to calculate actual values of the conductivity activation energy E_σ. A brief review on experimentally detected and actual values of E_σ is given by Stuke.[40] At this point it is useful to summarize the influence of thermal annealing on the dark conductivity of *p*-type amorphous suboxides derived from the results obtained so far: At annealing energies below 1.5–1.6 eV (regime I) a significant increase of the dark conductivity is observed. The physical origin of this activation of boron acceptors—and the corresponding shift of the Fermi level closer to the valence band edge—is most likely the dissociation of passivating boron-hydrogen complexes due to an effusion of hydrogen atoms. Alternatively, a small scale motion of hydrogen atoms at low annealing temperatures may occur. The activation of boron atoms is limited by a sudden effusion of a large quantity of weakly bound hydrogen and a concomitant phase separation of the amorphous suboxides. This leads to a sharp drop in the dark conductivity. Finally, partial crystallization occurs after all hydrogen has effused. This gives rise to a further activation of boron acceptors in the crystalline regions of the films.

E. Acceptor density in *p*-type suboxides

We would now like to discuss in more detail the conductivity activation observed for *p*-type samples at low annealing energies. We used the following equation to calculate the acceptor density N_A from conductivity values (electron charge *e*, free hole mobility $\mu = 1\ \text{cm}^2/\text{Vs}$).[41]

$$\sigma = e\mu N_A \exp(-E_\sigma / kT). \tag{4}$$

Hereby it is necessary to take into account the dependence of the conductivity activation energy $E_\sigma = E_F - E_V$ (valence-band energy E_V) on the varying acceptor density due to a shift of the Fermi energy, E_F. As is schematically shown in Fig. 15, activated dopants successively fill the states of the exponential bandtail of the amorphous suboxides and thus

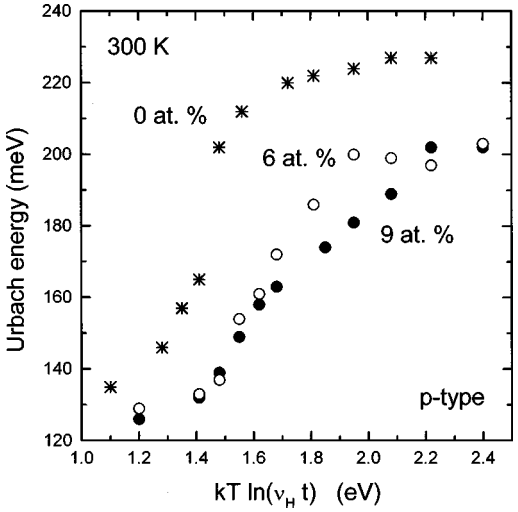

FIG. 16. Urbach energy of *p*-type suboxides with oxygen contents of 0, 6, and 9 at. % as a function of annealing energy.

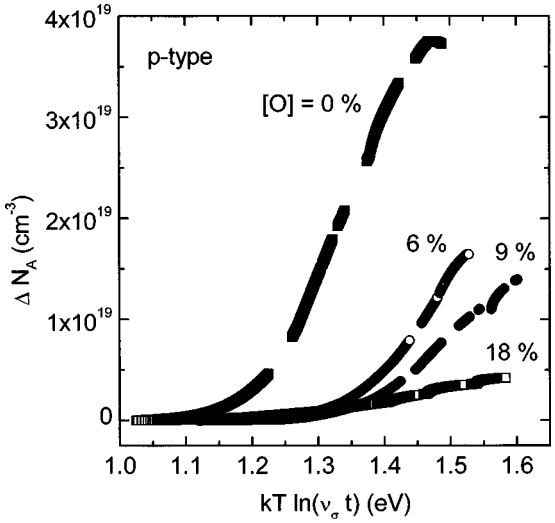

FIG. 17. Change in the acceptor density ΔN_A of *p*-type suboxides with oxygen contents of 0, 6, 9, and 18 at. % as a function of annealing energy. ΔN_A was calculated from dark conductivity values as described in the text.

shift the Fermi energy closer to the valence band. The necessary change in the dopant density ΔN_A can be calculated using

$$\Delta N_A = \int_{E_{F1}}^{E_{F2}} N(E)\,dE. \tag{5}$$

E_{F_1} is the initial Fermi energy level and $N(E)$ the energy dependant density of states. For the exponential Urbach tail we use

$$N(E) = 10^{21}\,\mathrm{cm}^{-3}\,\mathrm{eV}^{-1}\exp(-E/E_0). \tag{6}$$

Here $10^{21}\,\mathrm{cm}^{-3}\,\mathrm{eV}^{-1}$ is the value of the density of states at the band edge[42] and the Urbach energy E_0 describes the exponential slope of the valence band tail.

Using Eqs. (4), (5), and (6) it is possible to estimate the acceptor density N_A from conductivity values

$$N_A = (\sigma/e\mu)^{kT/(kT+E_0)}(10^{21}\,\mathrm{cm}^{-3}\,\mathrm{eV}^{-1}\,E_0)^{E_0/(kT+E_0)}. \tag{7}$$

We have to further take into account that the Urbach energy of amorphous suboxides is affected by thermal annealing. The Urbach energy was deduced from optical absorption measurements using photothermal deflection spectroscopy. The measurements were made at room temperature after consecutive annealing steps. It was assumed that the exponential increase of the absorption coefficient reflects the density of valence band tail states, as is commonly done for amorphous silicon.[42,43] Figure 16 shows the dependence of the Urbach energy on the annealing energy for *p*-type samples with 0, 6, and 9 at. % oxygen. Annealing increases the disorder of the amorphous films and leads to broader bandtails. The increase of the Urbach slope occurs at lower annealing energies for the sample with 0 at. % oxygen and reaches a significantly higher saturation value at large annealing energies. Onset and shape of the curves closely follow the dependency of the optical band gap on the annealing energy (see Fig. 5). It is therefore reasonable to assume that the effusion of hydrogen leads to an increase of the structural disorder of the films. Since the Urbach energy of the films increases during thermal annealing, the calculation of the acceptor density using Eq. (7) was done based on the experimental results in Fig. 16.

The value of the acceptor density in the as-deposited state $N_A(0)$ was calculated to be $1.6\times10^{19}\,\mathrm{cm}^{-3}$ for the *p*-type film with 0 at. % oxygen. $N_A(0)$ decreases with the incorporation of oxygen, being 1.4, 1.1, and $0.7\times10^{19}\,\mathrm{cm}^{-3}$ for the samples with 6, 9, and 18 at. % oxygen. With a dopant gas concentration of 1% we therefore observe doping efficiencies of 3% for 0 at. % oxygen and 1.5% for 18 at. % oxygen for our *p*-type samples prior to the thermal annealing. Similar values of the doping efficiency for a dopant gas concentration of 1% were reported by Stutzmann *et al.* for boron-doped *a*-Si:H.[44] Isothermal annealing of our films leads to an enhancement of the dark conductivity shown in Fig. 9. This is due to an activation of boron acceptors and gives rise to an increasing calculated acceptor density.

Figure 17 shows the change of the acceptor density ΔN_A as a function of the energy parameter $kT\ln(\nu_\sigma t)$ for *p*-type suboxides with various oxygen contents. Incorporation of oxygen increases the thermal energy at which the onset of the activation of boron was detected and reduces the maximum increase of the acceptor density. As we have shown by comparison of hydrogen effusion measurements and IR spectroscopy, a small scale motion of hydrogen atoms or an effusion of hydrogen, which is weakly bound, e.g., in Si-H_2 configurations, takes place at low annealing energies. This apparently leads to an increased incorporation of boron at electrically active sites, possibly due to a dissociation of passivating boron-hydrogen complexes. The shift of the onset of dopant activation to higher annealing energies with increasing oxygen content might thus be due to the stabilization of these passivating complexes by backbonded oxygen atoms.

An enhancement of the dark conductivity is achieved up to an amount of effused hydrogen of 2 at. %. Using an atomic density of $5\times10^{22}\,\mathrm{cm}^{-3}$ for amorphous silicon, this amounts to about $10^{21}\,\mathrm{cm}^{-3}$ effused hydrogen atoms. As we have mentioned earlier, approximately one out of ten effused hydrogen atoms influences the electrical properties of the

films. For our sample with 0 at. % oxygen the change of the acceptor density comprises $4\times10^{19}\,\mathrm{cm}^{-3}$ being roughly one order of magnitude lower than the effused hydrogen. Thus, thermal annealing at low annealing energies increases the acceptor density by up to a factor of three compared to the as-deposited films, giving rise to the observed enhancement of the dark conductivity (see Fig. 10). The opposite effect of a decreasing dark conductivity for boron-doped *a*-Si:H after a post hydrogenation plasma treatment was found by Magariño *et al.*[45] He attributed this effect to the creation of inactive, threefold coordinated boron atoms by the introduced hydrogen atoms. Increasing concentrations of oxygen in our films inhibits the activation of dopant atoms just as it reduces the probability of boron incorporation on electrically active sites during deposition. The microscopic origin of this effect is not fully understood, but it seems that increasing oxygen concentrations in amorphous silicon promotes the incorporation of inactive, threefold coordinated dopant atoms due to a larger flexibility of the amorphous network and the increased concentration of voids in the films.

We have shown that an optimized thermal annealing process at low annealing temperatures leads to a significant increase of the dark conductivity of *p*-type suboxides without affecting the optical bandgap. This is an important result, as the low conductivity of the *p* layers determines the series resistance of *p-i-n* light emitting devices. Moreover, the bandgap discontinuity at a *p-i*-interface governs the injection of holes into the *i*-layer. Thermal annealing of diode structures therefore causes a significant increase of the forward current density without inhibiting the carrier injection properties. Moreover, the dark conductivity and the optical band gap of *n*-type suboxides remain approximately unchanged at low annealing temperatures, so that the influence of thermal annealing on the *n* layers of *p-i-n* structures can be neglected.

IV. CONCLUSION

We have studied the effects of thermal annealing on the electronic properties of doped amorphous silicon suboxide films. For as-deposited samples efficient doping is possible up to $\sim$ 10 at. % oxygen in the films, where *p*- and *n*-type doping enhances the conductivity by three and six orders of magnitude, respectively. Thermal annealing of *p*-type suboxides at low annealing energies leads to conductivity activation due to an effusion of weakly bound hydrogen or a small scale motion of hydrogen in the films. This activation is less pronounced and shifts to higher annealing energies with increasing incorporation of oxygen in the films, but still increases the dark conductivity at 300 K by almost two orders of magnitude for *p*-type films with 9 at. % oxygen. Estimating the change in the acceptor density from conductivity data, we find that the effusion of approximately $10^{21}\,\mathrm{cm}^{-3}$ hydrogen leads to an activation of up to $4\times10^{19}\,\mathrm{cm}^{-3}$ boron atoms. No such conductivity activation was detected for *n*-type suboxides. The thermal conductivity activation of *p*-type suboxides is limited by the sudden effusion of a large quantity of weakly bound hydrogen, causing a major reconstruction of the amorphous network. At higher annealing temperatures the effusion of hydrogen bound in Si-H configurations causes a decrease of the optical band gap E_{04} and leads to a linear dependence of E_{04} on the hydrogen content of the amorphous suboxides, similar to what is known for *a*-Si:H. Optimized annealing thus is important to significantly improve the dark conductivity of *p*-type amorphous silicon suboxides. This has direct consequences for the fabrication of light emitting diodes, as the series resistance of these diodes is dominated by the high resistivity *p*-type layer.[5]

*Author to whom correspondence should be addressed. FAX: +49 89 289 12737. Electronic address: rainer.janssen@wsi.tu-muenchen.de

[1] M. Zacharias, H. Freistedt, F. Stolze, T. P. Drüsedau, M. Rosenbauer, and M. Stutzmann, J. Non-Cryst. Solids **164-166**, 1089 (1993).

[2] R. A. Street and J. C. Knights, Philos. Mag. B **42**, 551 (1980).

[3] M. C. Rossi, D. Dimova-Malinovska, M. S. Brandt, and M. Stutzmann, in *Inorganic and Organic Electroluminescence*, edited by R. H. Mauch and H.-E. Gumlich (Wissenschaft & Technik Verlag, Berlin, 1996), p. 189.

[4] W. Boonkosum, D. Kruangam, B. Ratwises, T. Sujaridchai, S. Panyakeow, S. Fujikake, and H. Sakai, J. Non-Cryst. Solids **198-200**, 1226 (1996).

[5] R. Janssen, U. Karrer, D. Dimova-Malinovska, and M. Stutzmann, J. Non-Cryst. Solids **227-230**, 1151 (1998).

[6] R. Carius, R. Fischer, E. Holzenkämpfer, and J. Stuke, J. Appl. Phys. **52**, 4241 (1981).

[7] E. Martinez and F. Indurain, Phys. Rev. B **24**, 5718 (1981).

[8] M. Zacharias, D. Dimova-Malinovska, and M. Stutzmann, Philos. Mag. B **73**, 799 (1996).

[9] W. Beyer, Physica B **170**, 105 (1991).

[10] W. Beyer, in *Tetrahedrally-Bonded Amorphous Semiconductors*, edited by B. Adler and H. Fritzsche (Plenum, New York, 1985), p. 129.

[11] R. A. Street, M. Hack, and W. B. Jackson, Phys. Rev. B **37**, 4209 (1987).

[12] M. Stutzmann, W. B. Jackson, and C. C. Tsai, Phys. Rev. B **32**, 23 (1985).

[13] M. Stutzmann and C. E. Nebel, in *Encyclopedia of Applied Physics*, edited by G. L. Trigg (VCH Publishers Inc. NY, 1997), Vol. 18, p. 151.

[14] B. von Roedern, L. Ley, and F. W. Smith, in *The Physics of Semiconductors*, edited by L. H. Wilson (IOP, London, 1978), p. 701.

[15] K. Haga, A. Murakami, K. Yamamoto, M. Kumano, and H. Watanabe, Jpn. J. Appl. Phys., Part 1 **30**, 3331 (1991).

[16] M. Zacharias, B. Garke, A. Panckow, H. Freistedt, and T. Drüsedau, in *Amorphous Silicon Technology*, edited by E. A. Schiff, M. J. Thompson, A. Madan, K. Tanaka, and P. G. Le Comber, MRS Symposia Proceedings No. 297 (MRS, Pittsburgh, 1993), p. 753.

[17] Y. Ichikawa, S. Fujikake, H. Ohta, T. Sasaki, and H. Sakai, in *Proceedings of the 22th IEEE Photovoltaik Conference, Las Vegas, 1991* (IEEE, NY, 1991), p. 1296.

[18] W. E. Spear and P. G. Le Comber, Solid State Commun. **17**, 1193 (1975).

[19] W. Beyer and H. Overhof, in *Semiconductors and Semimetals* (Academic, Orlando, 1984), Vol. 21C, Chap. 8, p. 257.

[20] Z. S. Jan, R. S. Bube, and J. C. Knights, J. Appl. Phys. **51**, 3278 (1980).

[21] K. Jiranapakul, K. Shirakawa, and J. Shirafuji, Jpn. J. Appl. Phys., Part 1 **25**, 1457 (1986).
[22] T. Shimizu, H. Kidoh, A. Morimoto, and M. Kumeda, Jpn. J. Appl. Phys., Part 1 **28**, 586 (1989).
[23] M. Isomura, T. Kinoshita, Y. Hishikawa, and S. Tsuda, Appl. Phys. Lett. **65**, 2329 (1994).
[24] M. Isomura, T. Kinoshita, and S. Tsuda, Appl. Phys. Lett. **68**, 1201 (1996).
[25] T. Shimizu, T. Ishii, M. Kumeda, and A. Masuda, J. Non-Cryst. Solids **227–230**, 403 (1998).
[26] W. M. Pontushka, W. W. Carlos, and P. C. Taylor, Phys. Rev. B **25**, 4362 (1982).
[27] M. C. Rossi, M. S. Brandt, and M. Stutzmann, in *Proceedings of the International Symposium on Advanced Luminescent Materials*, edited by D. J. Lockwood, P. M. Fauchet, N. Koshida, and S. R. J. Brueck (Pennington, NY, 1995), p. 445.
[28] M. C. Rossi, S. Salvatori, F. Galluzzi, R. Janssen, and M. Stutzmann, in Proceedings of the 9th International Conference on Modern Materials and Technologies-CIMTEC 98 (to be published).
[29] M. Cardona, Phys. Status Solidi B **118**, 463 (1983).
[30] G. Lucovsky, J. Non-Cryst. Solids **76**, 173 (1985).
[31] G. Lucovsky and W. B. Pollard, J. Vac. Sci. Technol. A **1**, 313 (1983).
[32] D. V. Tsu, G. Lucovsky, and B. N. Davidson, Phys. Rev. B **40**, 1795 (1989).
[33] G. Lucovsky, J. Tang, S. S. Chao, J. E. Tyler, and W. Czubatji, Phys. Rev. B **28**, 3225 (1983).
[34] K. Haga and H. Watanabe, J. Non-Cryst. Solids **195**, 2041 (1996).
[35] C. C. Tsai, Phys. Rev. B **19**, 2041 (1978).
[36] J. I. Pankove, P. J. Zanzucchi, C. W. Maggee, and G. Lucovsky, Appl. Phys. Lett. **46**, 421 (1985).
[37] N. M. Johnson, Phys. Rev. B **31**, 5525 (1985).
[38] Y. G. Du, Y. F. Zhang, G. G. Qin, and S. F. Weng, Solid State Commun. **55**, 501 (1985).
[39] N. F. Mott, Philos. Mag. **22**, 7 (1970).
[40] J. Stuke, J. Non-Cryst. Solids **97&98**, 1 (1987).
[41] T. Tiedje, J. Cebulka, D. Morel, and B. Abeles, Phys. Rev. Lett. **46**, 1425 (1981).
[42] K. Winer and L. Ley, in *Amorphous Silicon and Related Materials*, edited by H. Fritzsche (World Scientific, Singapore, 1988), p. 365.
[43] E. Bustarret, J. Non-Cryst. Solids **114**, 13 (1989).
[44] M. Stutzmann, D. K. Biegelsen, and R. A. Street, Phys. Rev. B **35**, 5666 (1987).
[45] J. Magariño, D. Kaplan, A. Friederich, and A. Deneuville, Philos. Mag. B **45**, 285 (1982).